Maksimainen, Mikko; Kurkela, Matti; Bhusal, Pramod; Hyyppä, Hannu

Calculation of Mesopic Luminance Using per Pixel S/P Ratios Measured with Digital Imaging

Published in:
Leukos

DOI:
10.1080/15502724.2018.1557526

Published: 02/10/2019

Document Version
Publisher's PDF, also known as Version of record

Taylor & Francis
Taylor & Francis Group

LEUKOS
The Journal of the Illuminating Engineering Society

ISSN: 1550-2724 (Print) 1550-2716 (Online) Journal homepage: http://www.tandfonline.com/loi/ulks20

Calculation of Mesopic Luminance Using per Pixel S/P Ratios Measured with Digital Imaging

Mikko Maksimainen, Matti Kurkela, Pramod Bhusal & Hannu Hyyppä

To cite this article: Mikko Maksimainen, Matti Kurkela, Pramod Bhusal & Hannu Hyyppä (2019): Calculation of Mesopic Luminance Using per Pixel S/P Ratios Measured with Digital Imaging, LEUKOS, DOI: 10.1080/15502724.2018.1557526

To link to this article: https://doi.org/10.1080/15502724.2018.1557526

Published online: 09 Jan 2019.

LEUKOS
https://doi.org/10.1080/15502724.2018.1557526

Calculation of Mesopic Luminance Using per Pixel S/P Ratios Measured with Digital Imaging

Mikko Maksimainen[a], Matti Kurkela[a], Pramod Bhusal[b], and Hannu Hyyppä[a]

[a]Department of Built Environment, Aalto University, Espoo, Finland; [b]Department of Electronics, Aalto University, PL 11000, 00076 AALTO, Espoo, Finland

ABSTRACT
This study describes a method of measuring the pixelwise S/P ratio using a calibrated digital camera and applying these S/P ratios to calculate mesopic luminance values. An example of using the developed method is presented. Further improvements for the method are discussed.

ARTICLE HISTORY
Received 28 March 2018
Revised 28 November 2018
Accepted 6 December 2018

KEYWORDS
Luminance imaging; mesopic vision; spectrum measurement

1. Introduction

Currently, a commonly used method for measuring the luminances of a visual environment is imaging luminance photometry. In imaging luminance photometry, a digital camera is utilized to measure luminances by interpreting the pixel red–green–blue (R, G, B) values as absolute luminances. In order to do this, the digital camera system is calibrated in terms of luminance and vignetting (Anaokar and Moeck 2005; Goldman and Chen 2005; Hiscocks 2013; Inanici 2006; Kim and Pollefeys 2008; Kurkela et al. 2017).

The human retina consists of cone cells used for accurate day and color vision and rod cells applied for dark vision. Day vision is also called "photopic vision," and dark vision is called "scotopic vision." The sensitivity peaks for photopic and scotopic visions are 555 nm and 507 nm, respectively (CIE 1990; Crawford 1949). Thus, scotopic vision is more sensitive to shorter wavelength (bluish) light, and photopic vision is more sensitive to longer wavelength (reddish) light. However, in the luminance range of 0.005–5.0 cd/m^2, partly scotopic and partly photopic vision applies (CIE 2010). This region is known as the "mesopic region," and the vision for this region is mesopic vision. In the CIE 191 system for mesopic photometry, the mesopic sensitivity curve is calculated as follows:

$$M(m)V_{mes}(\lambda) = mV(\lambda) + (1-m)V'(\lambda) \tag{1}$$

$$L_{mes} = \frac{683}{V_{mes(\lambda_0)}} \int V_{mes}(\lambda) L_e(\lambda) d\lambda \tag{2}$$

where m is the adaptation coefficient; $M(m)$ is a function that normalizes $V_{mes}(\lambda)$to a maximum value of 1; $V_{mes}(\lambda_0)$is the value of $V_{mes}(\lambda)$at 555 nm; $L_{mes}$is the mesopic luminance; $L_e(\lambda)$is the spectral radiance (W/m^{2}sr); when $L_{mes} \geq$ 5 cd/m^2, m = 1; when $L_{mes} \leq$ 0.005 cd/m^2, m = 0; The mesopic luminance, L_{mes}, and the coefficient, m, are calculated iteratively:

$$\begin{aligned} & m_0 = 0.5, \\ & L_{mes,n} = \frac{m_{(n-1)} L_p + \left(1 - m_{(n-1)}\right) L_s V'(\lambda_0)}{m_{(n-1)} + \left(1 - m_{(n-1)}\right) V'(\lambda_0)}, \\ & m_n = a + b * log_{10}\left(\frac{L_{mes,n}}{L_0}\right) \\ & \text{for } 0 \leq m_n \leq 1, \end{aligned} \tag{3}$$

where L_p is the photopic luminance; $L_s$is the scotopic luminance; $L_0$is 1 cd/m^2; and $V'(\lambda_0) = \frac{683}{1700}$ is the

CONTACT Mikko Maksimainen mikko.maksimainen@aalto.fi Department of Built Environment, Aalto University, PL 11000, 00076 AALTO, Espoo, Finland.

Color versions of one or more of the figures in the article can be found online at www.tandfonline.com/ULKS.

value of the scotopic spectral luminosity function when $\lambda_0 = 555$ nm; $a = 0.7670$; $b = 0.3334$; and n is the step of iteration (CIE 2010).

Mesopic photometry could be applied for more accurate measurement and optimized lighting design (Ylinen et al. 2011a). However, applying mesopic photometry is complicated. As mesopic photometry depends on the current state of retinal adaptation, and the adaptation luminance needs to be solved (Cengiz et al. 2015, 2016a; Maksimainen et al. 2016; Uchida and Ohno 2016a, 2016b). Furthermore, mesopic luminances depend on the spectral characteristics of the light and the surface reflecting the light (Bodrogi et al. 2015; He et al. 1998). Hence, a generalized model to apply mesopic photometry is very difficult to construct.

The S/P ratio is the ratio between radiation's scotopic and photopic spectral power distributions, and it can be calculated as follows:

$$S/P = \frac{1700\int_{380}^{760} \Phi_{e,\lambda} V'(\lambda) d\lambda}{683\int_{380}^{760} \Phi_{e,\lambda} V(\lambda) d\lambda} \tag{4}$$

where $\Phi_{e,\lambda}$ is the radiant power in watts for a certain wavelength, $V'(\lambda)$is the scotopic luminous efficiency curve, and $V(\lambda)$ is the photopic luminous efficiency curve.

Currently, only the S/P ratio of the light source is considered in mesopic photometry. However, the reflecting surfaces of the visual environment are often not neutral in terms of color. Thus, the colors of the surfaces influence the spectrum of the reflected light. Pavement stones and asphalt aggregate have different tones (Herold 2007; Preciado and Manzano 2017; Ylinen et al. 2011b). Obviously, the colors of the surrounding area also vary, from the painted surfaces of buildings to the colors of the vegetation.

Adaptation is a phenomenon where the retina adjusts to the amount of light in the visual environment (Moon and Spencer 1943, 1945). Adaptation mechanisms are disputed. In this study, adaptation is considered to be a local phenomenon on the retina (Cengiz et al. 2016b; Cleland and Enroth-Cugell 1968; Kastner and Baccus 2014; Meylan et al. 2007; Shapley and Enroth-Cugell 1984; Vangorp et al. 2015). Hence, we take a pixelwise approach to the adaptation luminance and mesopic luminance calculation. We do not try to estimate one global adaptation luminance value. Instead, we consider the Gaussian filtered local luminance of each pixel as its adaptation luminance.

One of the essential application areas for mesopic photometry is road lighting. International standards and recommendations regulate the road lighting design (European Committee for Standardization 2015; IES 2014). In the European CEN/TR 13201:2015 road lighting standard, only photopic luminance is considered. The ANSI/IES RP-8-14-recommended practice for roadway lighting mentions mesopic photometry. However, it only recommends the use of a simplified implementation for mesopic photometry, and only for off-road areas. Furthermore, the mesopic multiplier depends on the photopic adaptation luminance. Without a pragmatic solution to resolve the photopic adaptation luminance and the S/P ratio, the implementation of mesopic photometry will remain limited.

In this study, we introduce a pragmatic approach of imaging mesopic luminance photometry. The S/P ratios, adaptation luminances, and mesopic luminances are calculated for each pixel. A method for measuring the S/P ratios using a digital camera is introduced. Lastly, an example of using the imaging mesopic luminance photometry system is presented and the system's application areas are discussed.

2. Methods

As the imaging mesopic luminance photometer, we used a Nikon D800E camera with a Nikkor AF-S 14-24-mm f/2.8G ED objective. The camera had been calibrated in terms of luminance, vignetting, and geometric distortion (Kurkela et al. 2017). The Nikkor lens was locked to 14 mm, and the aperture and ISO sensitivity were f/5.6 and 100, respectively.

We developed a method to characterize the photometer sensor for an estimation of scotopic luminances. Eight different (A, B, C, D, E, F, G, and H) light emitting diode (LED) spectral reflections were measured from a Gigahertz-Optik ODM98 diffuse optical reflection surface with a Konica Minolta CS-2000 spectroradiometer. The diffused 12-channel LED panel was mounted directly above and in a parallel plane with the diffuse surface. The selection of LEDs in the panel consisted of neutral and cold white LEDs and 10 different narrowband LEDs, with dominant wavelengths of 453, 472, 497, 506, 527, 587, 596, 623, 636, and 662 nm. Simultaneously, the reflecting surface was captured with the Nikon D800E camera as illustrated in Fig. 1. The simultaneous measurements were captured from different directions. To ensure that the measurement direction had a tolerable effect, the spectra were measured using the spectroradiometer from directions −20°, 0°, and 20°. The relative difference of the spectra was 0.09% on average, which can be considered tolerable in terms of this study. The results can be found in Appendix A. To minimize the effect of vignetting, reflective surface was in the optical center of the image. Equation (4) was used to calculate the reference S/P ratios from the spectra measured with the spectroradiometer. Figure 2 illustrates the collection of spectra. The backgrounds for each spectrum are the linear images of the reflective surface captured using the Nikon D800E. The linear tagged image file (TIFF) images were converted from the raw Nikon Electronic Format (NEF) images applying the dcraw decoding program (DCRaw 2017). For this application, using linear images is a necessity. Each RGB value must be convertible into a luminance value linearly.

The S/P ratio was estimated from the captured luminance images. For the photopic factor, (5) was utilized (Hiscocks 2013). Scotopic factors were

Fig. 1. Method of capturing the spectra from the reflective surface using a Nikon D800E DSLR camera.

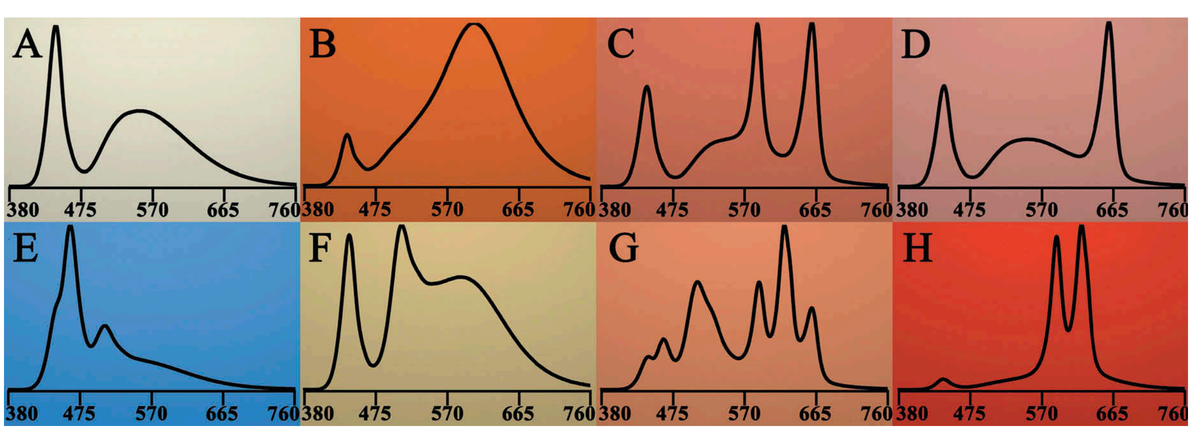

Fig. 2. (A)–(H) Eight normalized spectra visualized. The background of each spectrum is the linear image captured from the reflective surface.

derived summing the 1-nm bands of scotopic sensitivity curve within R, G, and B channels following the sRGB standard (International Electrotechnical Commission 1999). Hence, the normalized scotopic coefficients were 0.0070, 0.5190, and 0.4740 for R, G, and B respectively (6).

$$N_p = 0.2162R + 0.7152G + 0.0722B \qquad (5)$$

$$N_s = 0.0070R + 0.5190G + 0.4740B \qquad (6)$$

In order to calculate mesopic luminances, the state of retinal adaptation needs to be known. In high-dynamic-range imaging, the human visual system is approximated for tone reproduction by using a combination of a local pixel value and a global average or by calculating a local average with Gaussian or bilateral filtering (Reinhard et al. 2010). We applied the Gaussian filtering with kernel sizes of 25 and 251 to obtain the approximated adaptation luminances for each pixel. We also calculated the per pixel mesopic luminances without any filtering for the adaptation luminance.

The final procedure from measurement to estimated mesopic luminance image was as follows: capturing the raw image with imaging luminance photometer; applying DCRaw to obtain linear images in a TIFF format; applying the vignetting correction to the image; applying (5) to convert the R, G, and B values into absolute photopic luminances for each pixel; applying (6) to convert the R, G, and B values into absolute scotopic luminances for each pixel; calculating the S/P ratio for each pixel; Gaussian filtering the matrix of S/P ratios with the kernel size of 5 to reduce noise; approximating the adaptation luminances applying the table of photopic luminances, the table of photopic luminances that was Gaussian filtered with the kernel size of 25, and the table of photopic luminances that was Gaussian filtered with the kernel size of 251 for comparison; and calculating the state of adaptation for each pixel with (1), (2), and (3) using the Gaussian filtered matrix of adaptation luminances as the photopic luminances in the equation; calculating the pixel-wise mesopic luminances with one iteration round of (3), using th $m_{(n)}$ in the previous phase as the state of adaptation. The mesopic luminance calculation was performed applying a Python program. Figure 3 illustrates the procedure.

Here we present an example process for a single pixel. In 16-bit linear TIFF, the pixel has R, G, and B values of 5206, 3568, and 1798, respectively. This RGB value converted into a relative luminance value with (5) is 3807.1864, and multiplying this value by a calibration factor (0.000333135) results in an absolute photopic luminance value of 1.268 cd/m^2. Calculating the scotopic luminance from the same pixel with (6) results in a relative scotopic luminance value of 2740.4860 and, thus, we can calculate the S/P ratio (4) for that pixel (1700 * 2740.4860)/(683 * 3807.1864) ≈1.792. After applying Gaussian filtering with a kernel size of 5 to reduce noise in the table of all per pixel S/P ratios, the S/P ratio for this pixel obtained the value 1.838. Moreover, applying Gaussian filtering with a kernel size of 25 for the matrix of photopic luminances, we obtained an adaptation luminance value of 1.319 cd/m^2 for the pixel. Applying (1), (2), and (3)

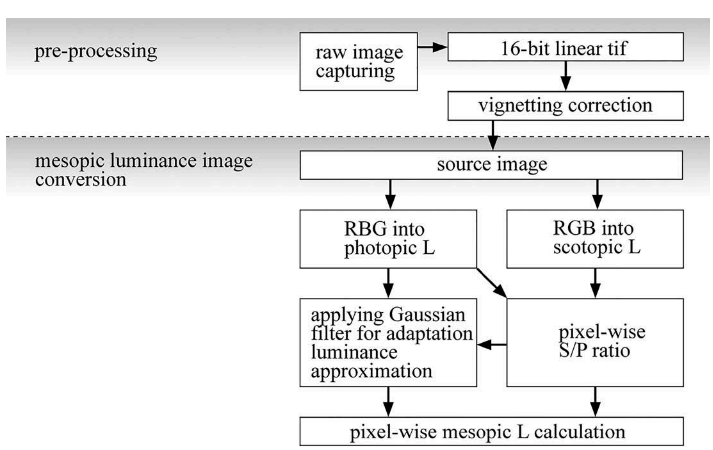

Fig. 3. Flowchart of the image processing and mesopic luminance calculation.

for six iteration rounds recursively to the adaptation luminance, we obtain an $m_{(n)}$ value of 0.8168. Finally, doing one more recursion of (3) with an $m_{(n)}$ value 0.8168 from the adaptation luminance but for the measured photopic luminance value, we obtain a mesopic luminance value of 1.356 cd/m^2.

3. Results

Table 1 presents the reference S/P ratios measured and calculated with the spectrophotometer in comparison with the S/P ratios estimated using the camera.

As an experimental case, we used a road section in Munkkiniemenranta, Helsinki. This example demonstrates the principle of the measurement concept. The street was illuminated with LED luminaires (AEC Illuminazione SRL LIN-1B-ST-075 LED-in 1B ST 4.5–63), whose S/P ratio, measured in a laboratory using a spectroradiometer (Konica Minolta CS-2000), was 1.42. We captured a luminance image in a way similar to that used for road lighting measurements. For a calculation area, we chose the section of the road surface illustrated in Fig. 4.

Figure 4 illustrates the measured street, the false-colored photopic luminance image, the false-colored mesopic luminance image (S/P ratio from laboratory measurement), and the false-colored mesopic luminance image (S/P ratio derived pixelwise with the estimation method).

With only visual assessment on the pseudocolored luminance images, differences appear to be nonexistent. However, the average luminances for the areas of analysis were 1.28 (1.2812), 1.44 (1.4355), and 1.58 (1.5768) cd/m^2 for the photopic measurement, the mesopic measurement with a fixed S/P ratio of the luminaire (1.42), and the mesopic measurement with pixelwise S/P ratio (average 1.805), respectively. Hence, compared to photopic luminances, the average mesopic luminances were 12.0% higher with the fixed S/P ratio and 23.1% higher with the pixelwise S/P ratio. The Gaussian filter used in the table of adaptation luminances had no effect on the mean values calculated from the area of measurement.

4. Discussion

With the iterated values for scotopic conversion, the S/P ratios of the tested set of spectral power distributions were solved with an average relative difference of 41%. The S/P ratios measured with the spectrophotometer were 1.99, 1.12, 4.11, 1.41, 1.85, 2.02, 2.04, and 0.54, and the respective S/P ratios measured with the camera were 2.38, 1.55, 3.22, 1.90, 2.19, 2.14, 1.94, and 1.07. The spectral power distribution cannot be presented using only three channels without losing information. Hence, the accuracy of this simplified measurement system will be limited. In the illustrative example case, the measurement system performed very well in terms of S/P ratio measurement. The S/P ratio measured from the street surface in the field with the camera was 1.41 and the S/P ratio measured in the laboratory for the same type of luminaire was 1.81. However, on the road surface, the color of the asphalt has an effect on the S/P ratio. This effect is always missing when calculating mesopic luminances using only the S/P ratio of the light itself. In this study, the mesopic luminances were calculated three times using three different tables of adaptation luminances. The first table was the calculated photopic luminances of the measurement, the second table was the photopic luminances filtered applying a Gaussian filter with a kernel size of 25, and the third table

Table 1. S/P ratios measured with a Konica Minolta CS-2000 and Nikon D800E and the relative difference between these two ratios.

Spectrum	S/P ratio with the CS-2000	S/P ratio with the Nikon D800E	Relative difference (%)
A	1.99	2.38	39
B	1.12	1.55	43
C	4.11	3.22	89
D	1.41	1.90	50
E	1.85	2.19	34
F	2.02	2.14	12
G	2.04	1.94	10
H	0.54	1.07	53
Average			41

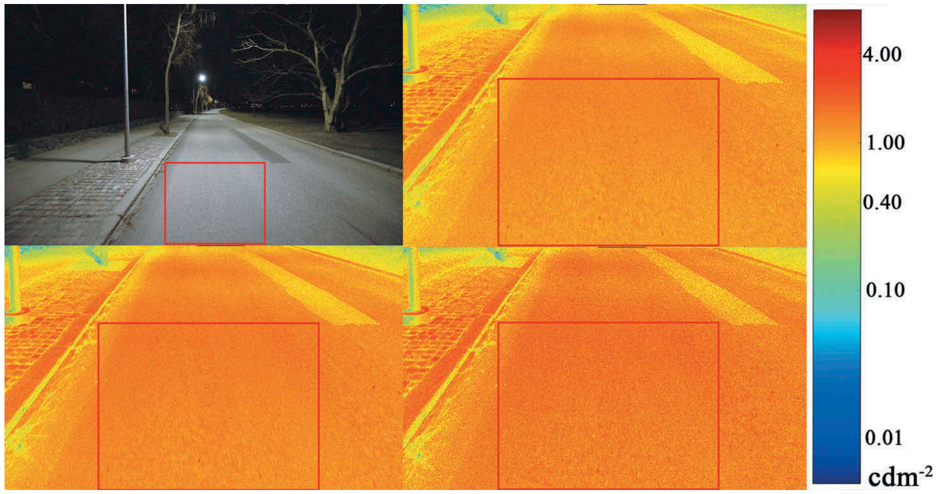

Fig. 4. (Top left) The measured street, (top right) the false-colored photopic luminance values, (bottom left) the false-colored mesopic luminance values calculated with the luminaire manufacturer's S/P ratio, and (bottom left) the false-colored mesopic luminance values calculated with the pixelwise S/P ratios. The red rectangle encompasses the area of analysis.

was the photopic luminances filtered applying a Gaussian filter with a kernel size of 251. The Gaussian filtering of the adaptation luminances had no measurable effect on the calculated mean mesopic luminance in the area of measurement.

We encourage experimenting with this concept of imaging S/P measurement and imaging mesopic luminance photometry. The accuracy of the measurement system could possibly be improved if a larger set of sampled spectra were used, and both the photopic and scotopic conversion coefficients were empirically characterized for the measurement system. Moreover, it would be more meaningful to reproduce the measurement system using a camera that can capture an image with better wavelength resolution than only R, G, and B channels. These kinds of cameras are called "hyperspectral cameras" or "imaging spectrographs," and they can measure the spectrum in, for example, 10-nm wavelength bands (Goetz et al. 1985; Gowen et al. 2007; Monteiro et al. 2007). Similar implementation of hyperspectral photometry may also be possible with consumer digital cameras (Lebourgeois et al. 2008; Solli et al. 2005b, 2005a). The spatial resolution of an imaging spectrograph is smaller than the spatial resolution of a digital single-lens reflex (DSLR) camera such as the Nikon D800E used in this study. However, it might be beneficial to sacrifice some spatial resolution to gain some spectral resolution when creating an imaging mesopic luminance photometer.

The second improvement to the measurement system would be to implement the cone and rod cell distribution functions pixelwise to the image. Thus, we could calculate the mesopic luminances in the right proportions and only to the retinal area where rod and cone cells coexist (Cursio et al. 1990; Osterberg 1935; Watson 2014). To implement the photoreceptor density functions correctly, the current fixation point must be predicted (Cengiz et al. 2013; Winter et al. 2016a, 2016b).

5. Conclusion

In this study, we present a concept of imaging S/P ratio and mesopic luminance measurement. Furthermore, we presented that approachable imaging mesopic luminance meters are able to be developed and the pixelwise computations are feasible. It is debatable as to whether it would be better to use the S/P ratio of the light source that does not take the color of the surface into account or the pixelwise S/P ratio of the reflected light estimated with the digital camera sensor response figures. However, the effect of chromaticity in the visual environment can only be measured with imaging photometry. Hence, the measurement concept presented in this study can be the best compromise for certain applications.

The mechanisms of adaptation remain as the primary difficulty in the mesopic luminance calculation process. The adaptation luminance of the peripheral vision is especially difficult to determine. Moreover, within a constantly changing visual environment, the latencies related to simultaneously occurring mechanical, chemical, and neurological luminance adaptations affect the adaptation luminance. The measurement system presented in this study is applicable if adaptation is considered mainly local and instantaneous. Once we learn more about peripheral adaptation, optimized filtering can be applied to each pixel within a certain solid angle and location in the visual field.

Disclosure statement

No potential conflict of interest was reported by the authors.

Funding

This work was supported by the Academy of Finland, the Centre of Excellence in Laser Scanning Research (CoE-LaSR; Grants 272195, 307362). The Strategic Research Council at the Academy of Finland is acknowledged for financial support for project “Competence Based Growth through Integrated Disruptive Technologies of 3D Digitalization, Robotics, Geospatial Information and Image Processing/Computing—Point Cloud Ecosystem (293389, 314312),” and the European Regional Development Fund “Leverage from the EU 2014–2020” supported this work under project “3D Cultural Hub” (Grant A72980).

References

Anaokar S, Moeck M. 2005. Validation of high dynamic range imaging to luminance measurement. LEUKOS. 2:133–44.

Bodrogi P, Schiller C, Khanh TQ. 2015. Testing the CIE system for mesopic photometry in a threshold detection experiment. Light Res Technol. 48(8):992–1004.

Cengiz C, Kotkanen H, Puolakka M, Lappi O, Lehtonen E, Halonen L DSc, Summala H. 2013. Combined eye-tracking and luminance measurements while driving on a rural road: towards determining mesopic adaptation luminance. Light Res Technol. 46(6):676–94.

Cengiz C, Maksimainen M, Puolakka M, Halonen L. 2015. Contrast threshold measurements of peripheral targets in night-time driving images. Light Res Technol. 48(4):491–501.

Cengiz C, Maksimainen M, Puolakka M, Halonen L. 2016a. Contrast threshold measurements of peripheral targets in night-time driving images. Light Res Technol. 48:491–501.

Cengiz C, Maksimainen M, Puolakka M, Halonen L. 2016b. The effects of high luminance objects on peripheral target detection in mesopic conditions. Light Eng. 24(1):12–20.

Cleland BG, Enroth-Cugell C. 1968. Quantitative aspects of sensitivity and summation in the cat retina. J Physiol. 198 (1):17–38.

[CIE] Commission International de l’Éclairage. 2010. Recommended system for mesopic photometry based on visual performance. Vienna (Austria): CIE. CIE Publication 191; p. 79.

[CIE] Commission Internationale de l’Eclairage. 1990. CIE 1988 2° Spectral luminous efficiency function for photopic vision. CIE Publication No. 86. doi:10.1099/00221287-136-2-327

Crawford BH. 1949. The scotopic visibility function. Proc Phys Soc Sec B. 62(5):321–34.

Curcio CA, Sloan KR, Kalina RE, Hendrickson AE. 1990. Human photoreceptor topography. J Comp Neurol. 292:497–523.

DCRaw. 2017. Decoding raw digital photos in Linux. Available online: http://www.webcitation.org/6rVWV6dQ3 (archived on 26th June 2017).

European Committee for Standardization. 2015. Road lighting—Part 1: guidelines on selection of lighting classes. CEN/TR 13201-1. Brussels (Belgium).

Goetz AFH, Vane G, Solomon JE, Rock BN. 1985. Imaging spectrometry for Earth remote sensing. Science. 228 (4704):1147–53.

Goldman DB, Chen J-H 2005. Vignette and exposure calibration and compensation. Proceedings of Tenth IEEE International Conference on Computer Vision (ICCV’05), Beijing, China, 15 – 21 October 2005, 899–906. doi:10.1109/ICCV.2005.249.

Gowen AA, O’Donnell CP, Cullen PJ, Downey G, Frias JM. 2007. Hyperspectral imaging – an emerging process analytical tool for food quality and safety control. Trends Food Sci Technol. 18(12):590–98.

He Y, Bierman A, Rea MS. 1998. A system of mesopic photometry. Light Res Technol. 30(4):175–81.

Herold M. 2007. Spectral characteristics of asphalt road surfaces. In: Remote sensing of impervious surfaces. Boca Raton (FL): CRC Press; p. 237–47.

Hiscocks PD 2013. Measuring luminance with a digital camera: case history. <http://www.ee.ryerson.ca:8080/~phiscock/astronomy/light-pollution/luminance-case-history.pdf> Accessed 2018 March 28th.

[IES] Illuminating Engineering Society of North America. 2014. American standard practice for roadway lighting. IESNA RP-8-14. New York (NY).

Inanici MN. 2006. Evaluation of high dynamic range photography as a luminance data acquisition system. Light Res Technol. 38:123–34.

International Electrotechnical Commission. 1999. Multimedia systems and equipment - Colour measurement and management - Part 2-1: colour management - Default RGB colour space – sRGB. IEC 61966-2-1:1999. Geneva (Switzerland).

Kastner DB, Baccus SA. 2014. Insights from the retina into the diverse and general computations of adaptation, detection, and prediction. Curr Opin Neurobiol. 2014(25):63–69.

Kim SJ, Pollefeys M. 2008. Robust radiometric calibration and vignetting correction. IEEE Trans Pattern Anal Mach Intell. 30:562–76.

Kurkela M, Maksimainen M, Vaaja MT, Virtanen J-P, Kukko A, Hyyppä J, Hyyppä H 2017. Camera preparation and performance for 3D luminance mapping of road environments. Photogramm J Finland. 25(2). doi:10.17690/017252.1

Lebourgeois V, Bégué A, Labbé S, Mallavan B, Prévot L, Roux B. 2008. Can commercial digital cameras be used as multispectral sensors? A crop monitoring test. Sensors. 8(11):7300–22.

Maksimainen M, Puolakka M, Tetri E, Halonen L. 2016. Veiling luminance and visual adaptation field in mesopic photometry. Light Res Technol. 49(6):743–62.

Meylan L, Alleysson D, Süsstrunk D. 2007. Model of retinal local adaptation for the tone mapping of color filter array images. J Opt Soc Am A. 24:2807–16.

Monteiro ST, Minekawa Y, Kosugi Y, Akazawa T, Oda K. 2007. Prediction of sweetness and amino acid content in soybean crops from hyperspectral imagery. ISPRS J Photogramm Remote Sens. 62(1):2–12.

Moon P, Spencer DE. 1943. The specification of foveal adaptation. J Opt Soc Am. 33(8):444–56.

Moon P, Spencer DE. 1945. The visual effect of non-uniform surrounds. J Opt Soc Am. 35(3):233–48.

Osterberg GA. 1935. Topography of the layer of rods and cones in the human retina. Acta Ophthalmol (Copenh). 6:1–102.

Preciado OU, Manzano ER. 2017. Spectral characteristics of road surfaces and eye transmittance: effects on energy efficiency of road lighting at mesopic levels. Light Res Technol. doi:10.1177/1477153517718227

Reinhard E, Heidrich W, Debevec P, Pattanaik S, Ward G, Myszkowski K. 2010. High dynamic range imaging: acquisition, display, and image-based lighting. 2nd ed. Burlington (MA): Morgan Kaufmann.

Shapley R, Enroth-Cugell C. 1984. Visual adaptation and retinal gain controls. Progress in retinal research, Vol 3. Oxford (UK): Pergamon Press; p. 358. doi:10.1016/0039-6257(85)90064-5

Solli M, Andersson M, Kruse B, Lenz R 2005b. Digital camera characterization for color measurements. Proceedings of 2005 Beijing International Conference on Imaging: Technology and Applications for the 21st Century. Beijing (China); pp 278–79.

Solli M, Andersson M, Lenz R, Kruse B 2005a. Color measurements with a consumer digital camera using spectral estimation techniques. Image Analysis, SCIA, Proceedings of 14th Scandinavian Conference, Finland. pp 105–14. doi:10.1007/11499145_12.

Uchida T, Ohno Y. 2016a. Defining the visual adaptation field for mesopic photometry: effect of surrounding source position on peripheral adaptation. 2016. Light Res Technol. 49(6):763–73.

Uchida T, Ohno Y. 2016b. Simplified field measurement methods for the CIE mesopic photometry system. Light Res Technol. 49(6):774–87.

Vangorp P, Myszkowski K, Graf EW, Mantiuk RK. 2015. A model of local adaptation. ACM Trans Graph. 34(6):166. doi:10.1145/2816795.2818086. 1–166: 13.

Watson AB. 2014. A formula for human retinal ganglion cell receptive field density as a function of visual field location. J Vis. 14(7):15,1–17.

Winter J, Fotios S, Völker S. 2016a. The effects of glare and inhomogeneous visual fields on contrast detection in the context of driving. Light Res Technol. doi:10.1177/1477153516672719

Winter J, Fotios S, Völker S. 2016b. Gaze direction when driving after dark on main and residential roads: where is the dominant location? Light Res Technol. 49(5):574–85.

Ylinen A-M, Pellinen T, Valtonen J, Puolakka M, Halonen L. 2011b. Investigation of pavement light reflection characteristics. Road Mater Pavement Des. 12(3):587–614.

Ylinen A-M, Tähkämö L, Puolakka M, Halonen L. 2011a. Road lighting quality, energy efficiency, and mesopic design – LED street lighting case study. Leukos. 8 (1):9–24.

Appendix A

The spectra of cool white and warm white LEDs measured with a Konica Minolta CS-2000 spectroradiometer from angles −20°, 0°, and 20°. The target was a diffuse Gigahertz-Optik ODM98 diffuse optical reflection surface (Figs. A1 and A2).

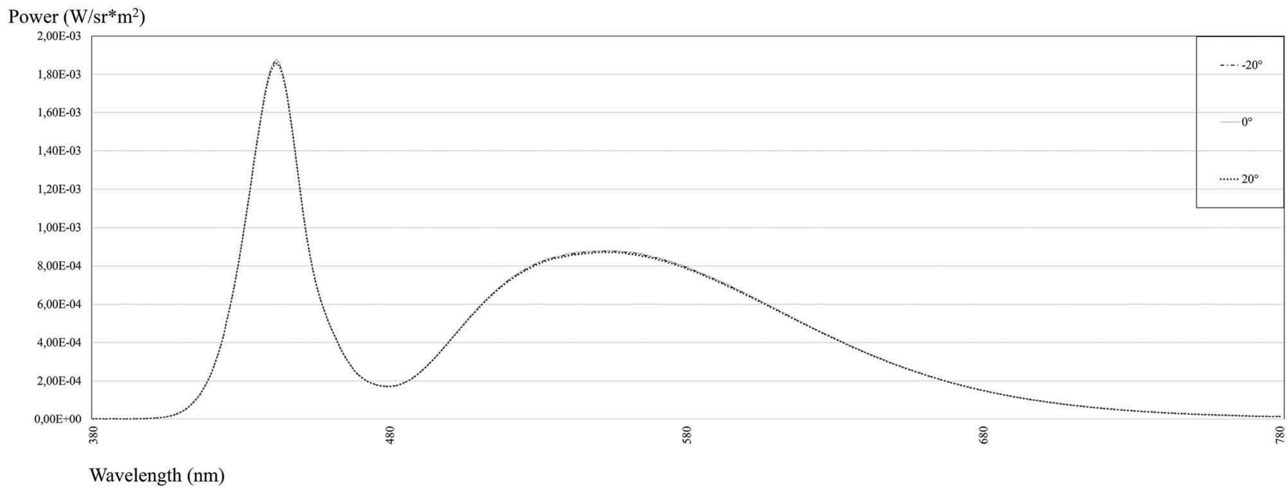

Fig. A1. Power [W/(sr*m^2)] as a function of wavelength (nm), cool white LED.

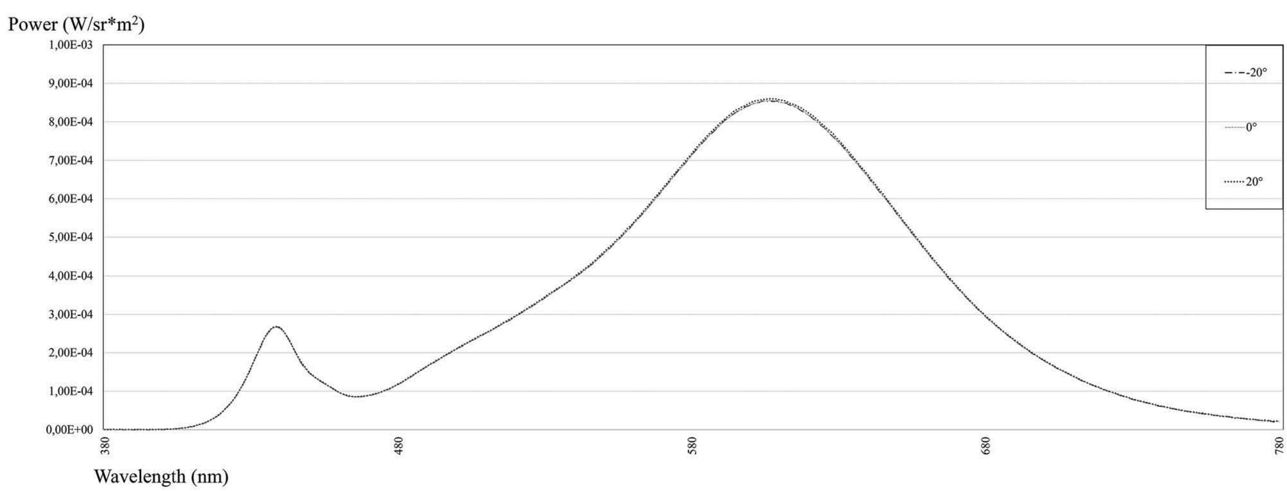

Fig. A2. Power [W/(sr*m^2)] as a function of wavelength (nm), warm white LED.